Hosing Instability in the Blow-Out Regime for Plasma-Wakefield Acceleration

C. Huang,[1] W. Lu,[1] M. Zhou,[1] C. E. Clayton,[1] C. Joshi,[1] W. B. Mori,[1] P. Muggli,[2] S. Deng,[2] E. Oz,[2] T. Katsouleas,[2] M. J. Hogan,[3] I. Blumenfeld,[3] F. J. Decker,[3] R. Ischebeck,[3] R. H. Iverson,[3] N. A. Kirby,[3] and D. Walz[3]

[1]*University of California, Los Angeles, California 90095, USA*
[2]*University of Southern California, Los Angeles, California 90089, USA*
[3]*Stanford Linear Accelerator Center, Menlo Park, California 94025, USA*

The electron hosing instability in the blow-out regime of plasma-wakefield acceleration is investigated using a linear perturbation theory about the electron blow-out trajectory in Lu *et al.* [in Phys. Rev. Lett. **96**, 165002 (2006)]. The growth of the instability is found to be affected by the beam parameters unlike in the standard theory Whittum *et al.* [Phys. Rev. Lett. **67**, 991 (1991)] which is strictly valid for preformed channels. Particle-in-cell simulations agree with this new theory, which predicts less hosing growth than found by the hosing theory of Whittum *et al.*

Recent experiments have shown amazing progress for both plasma-wakefield acceleration (PWFA) and laser wakefield acceleration (LWFA) [1–3] in the electron blow-out regime. In this regime, plasma electrons are completely evacuated by the space charge force of an electron beam or the ponderomotive force of a laser pulse, forming an ion channel on the axis of the system with a laminar sheath at the channel boundary carrying large concentrations of relativistic electrons. However, the electron hosing instability [4–7] of the drive and/or trailing beam remains a major concern for PWFA/LWFA concepts. The hosing instability results from the interaction between the electron sheath and the self-injected or externally injected electron beam. It leads to spatiotemporally growing oscillations of the beam centroid at each axial slice thus limiting the useful acceleration length and making it difficult to aim the beam. Existing standard theory [4,6] predicts rapid growth for this instability. However, recent experiments [1,2] have shown little evidence of hosing.

In this Letter, we present a more general hosing theory based on a perturbation method to the zeroth order trajectory [8] for the ion-channel/electron-sheath boundary. The initial hosing growth predicted by the linearized coupling is found to be affected by the nonconstant channel radius, relativistic mass corrections, and the longitudinal velocity of electrons in the plasma sheath. We verify this theory using particle-in-cell (PIC) simulations and compare it to the standard theory.

The existing work [4,6] focused on the hosing in a long ion channel with a radius near the charge neutralization radius, i.e., $r_c \sim r_{\rm neu} = \sqrt{n_b R_b^2/n_p}$, where n_b, n_p are the beam and plasma density, respectively, and R_b is the beam radius. Such a channel is either preformed or adiabatically formed. The electrons in the sheath layer are assumed to be at rest, i.e., the nonrelativistic limit; therefore, they do not generate or feel the magnetic fields. This adiabatic (referring to the channel formation), nonrelativistic (referring to the plasma sheath motion) limit is appropriate for a beam with a long bunch length $L \gg \lambda_p$ and weak charge per unit length $\Lambda = k_p^2 r_{\rm neu}^2 = 4I_b/I_A \ll 1$, where $k_p = \omega_p/c$, $\omega_p = \sqrt{4\pi n_p e^2/m}$, $\lambda_p = 2\pi k_p^{-1}$ are the wave number, angular frequency, and wavelength of the plasma wave moving at the speed of light, and I_b and $I_A = 17$ kA are the beam and Alfvén current, respectively. Such a beam creates a long channel with radius $r_c \approx r_{\rm neu} \ll k_p^{-1}$; therefore, the plasma sheath is nonrelativistic. In this limit, the linearized coupled equations for the channel centroid x_c and the beam centroid x_b are [4,7]

$$\partial_s^2 x_b + k_\beta^2 x_b = k_\beta^2 x_c, \qquad \partial_\xi^2 x_c + \omega_0^2 x_c = \omega_0^2 x_b, \quad (1)$$

where $k_\beta = k_p/\sqrt{2\gamma}$, $\omega_0 = k_p/\sqrt{2}$, s is the propagation distance into the plasma, $\xi = ct - z$ is the location within the beam, and γ is the beam Lorentz factor. For a PWFA, the ''short-pulse'' limit of these equations is relevant, i.e., $k_\beta s \gg \omega_0 \xi$, and the asymptotic solution for a linear tilt in x_b is $x_b/x_{b0} = 0.341 A^{-3/2} e^A \cos(k_\beta s - A/\sqrt{3} + \pi/4)$ [6], where $A = 1.3[(k_\beta s)(\omega_0 \xi)^2]^{1/3}$. In this short-pulse regime $\partial_\xi^2 x_c \gg \omega_0^2 x_c$ and x_b oscillates nearly resonantly in s with a wave number k_β.

In this Letter we investigate how the physics of the short-pulse asymptotic behavior is modified when the channel is formed nonadiabatically and when relativistic mass corrections arise (i.e., $L < \lambda_p$, $\Lambda > \sim 1$, and $r_{c,\max} > k_p^{-1}$). Under these conditions, the variation of r_c along the beam is not negligible and the motion in the electron sheath can be relativistic. And using a fully explicit 3D simulation [9], hosing was found to be less severe than the standard theory prediction. The reasons for the reduced growth rate were not then clearly identified. Here we identify the physics that reduces the growth rate and quantify their effects.

We first illustrate how hosing occurs in the nonadiabatic, relativistic blow-out regime using a 3D fully nonlinear PIC code, QuickPIC [10], which uses the quasistatic approximation as discussed just after Eq. (2) below. Figure 1(a)

Submitted to Phys.Rev.Lett.

Work supported in part by US Department of Energy contract DE-AC02-76SF00515

shows the beam after the hosing instability has developed and saturated in the simulation. In Fig. 1(b) the centroid of the beam at the location of the left-hand (blue) arrow is plotted and compared to the asymptotic solution from the standard theory. The simulation parameters are as follows [9]: $n_p = 2\times10^{16}$ cm^{-3}, $n_b/n_p = 25.9$, $k_p\sigma_r = 0.19$, $k_p\sigma_z = 1.2$, where σ_r and σ_z are beam RMS radius and length, respectively. The beam has an initial linear tilt of angle $\Theta = 0.011$.

There are three regions along the beam which exhibit different behavior as indicated in Fig. 1(a) by the (yellow) box, left-hand (blue) arrow, and right-hand (green) arrow, respectively. In region I the ion channel has not yet completely formed and the latter part of the head gradually aligns with the front of the beam. In region II, the ion channel is fully formed and the electron sheath is laminar. Recently, Lu *et al.* [8] showed that the channel shape in this region can be represented by the trajectory of an electron at the channel boundary, defined as $r_0(\xi)$. We label the upper and lower trajectories as r_+ and r_-, respectively. For a beam without a tilt, $r_+ = r_- = r_0$. The linear (described by linearized equations) and nonlinear stages of hosing are seen in the lower red curve in Fig. 1(b) before and after $0.65m$, respectively. In region III, the hosing amplitude becomes comparable to the channel radius and the beam breaks apart when it hits the channel boundary.

In this Letter, the linear stage of hosing growth in region II is studied. Clearly any theory for hosing of short pulses needs to include channel formation. (Our theory should also be valid when the plasma is created by self-ionization from the drive beam when the diameter of the ionized gas, $d \gg 2r_c$. The opposite limit where $d \le 2r_c$ was studied in [11].) A perturbative model to the electron trajectory at the channel boundary is developed for small hosing amplitudes. To lowest order, the charge and current density perturbations at the boundary can be approximated as dipoles by a slightly shifted channel.

We use the coordinates $(x, y, s = z, \xi = ct - z)$ with xz being the hosing plane and assume a quasistatic plasma response which essentially means that the s dependence

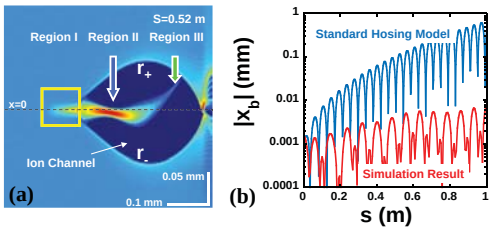

FIG. 1 (color). (a) A 2D slice of the beam (moving to the left) and plasma density after the beam has propagated 0.52 m, illustrating the three regions of behavior. (b) The beam centroid $|x_b|$ (lower red curve) in the simulation (the asymmetry in this curve is due to beam centroid aligning to the axis at region I) and from the standard theory prediction (upper blue curve). The growth in the simulation is 1 order of magnitude smaller than the standard theory prediction.

(except for that due to beam evolution) is removed when calculating the electron trajectory. The perturbation to the zeroth order trajectory is assumed to be small. Also, the focusing force is still assumed to be linear in r, i.e., channel deformation is omitted. The channel centroid can be defined as $x_c(\xi) = [r_+(\xi) - r_-(\xi)]/2$. The channel diameter $d = r_+ + r_-$ is also assumed to be unchanged. Furthermore, the beam is assumed to be axisymmetric and narrow compared to r_0, so beam deformation can be neglected. Therefore, the coupling from the channel to the beam centroid x_b is treated the same way as in [4].

Based on these assumptions, we derive a new equation for the channel centroid from the relativistic radial equation of motion for a plasma electron, beginning from what is essentially Eq. (3) of [8] but with no laser field

$$\frac{dP_\perp}{dt} = \frac{d}{dt}\left(\gamma\frac{dr}{dt}\right) = -(E_r - V_z B_\theta), \tag{2}$$

where $P_\perp$, V_z are the perpendicular (radial) momentum and longitudinal velocity of a plasma electron, and E_r and B_θ are the self-consistent radial electric field and azimuthal magnetic field, respectively. We normalize mass to m, charge to e, velocities to the speed of light c, lengths to k_p^{-1}, densities to n_p, and fields to $mc\omega_p/e$. Under the quasistatic approximation, $\gamma(1 - V_z) = 1 + \psi$ [12], or $\gamma = [1 + P_\perp^2 + (1+\psi)^2]/2(1+\psi)$, where the potential $\psi \equiv \phi - A_z$ is the solution to the Poisson equation $-\nabla_\perp^2\psi = 4\pi(\rho - J_z)$ in Lorentz gauge, and ρ, J_z are plasma charge and longitudinal current densities, respectively. Thus $d/dt = (1 - V_z)d/d\xi = (1+\psi)d/(\gamma d\xi)$ and $P_\perp = \gamma dr/dt = (1+\psi)dr/d\xi$. So Eq. (2) becomes (we define $d/d\xi \equiv {}'$)

$$(1+\psi)[(1+\psi)r']' = -\gamma(E_r - V_z B_\theta). \tag{3}$$

When the beam is straight, i.e., unperturbed, the solution to Eq. (3) is defined as $r_0(\xi)$ with other unperturbed quantities being E_0, B_0, ψ_0, $V_0(\xi)$, and $\gamma_0(\xi)$, respectively (subscripts r, z, and θ are dropped). Next, perturbations with subscript "1" are introduced.

$$r = r_0 + r_1, \qquad V = V_0 + V_1, \tag{4}$$

$$E = E_0 + E_1, \qquad B = B_0 + B_1, \tag{5}$$

$$\psi(r_0 + r_1) \approx \psi_0(r_0), \text{ i.e., } \psi_1 \approx 0. \tag{6}$$

Equation (6) follows from the assumption that the channel is simply displaced by r_1 without deformation and the fact that ψ is insensitive to the change in the profile of $(p - J_z)$ [8]. Equation (6), together with $\gamma = [1 + P_\perp^2 + (1+\psi)^2]/2(1+\psi)$ and $P_\perp = (1+\psi)r'$, leads to $\gamma = \gamma_0 + \gamma_1 = \gamma_0 + (1+\psi_0)r_0'r_1'$. By substituting γ and Eqs. (4)–(6) into Eq. (3) and ordering the resulting terms, we obtain the zeroth order Eq. (7) and first order Eq. (8),

$$(1+\psi_0)[(1+\psi_0)r_0'' + \psi_0' r_0'] = -\gamma_0(E_0 - V_0 B_0) \tag{7}$$

TABLE I. Simulation parameters, and $\gamma = 55, 773$ for each case.

Parameter	Simulation (a)	Simulation (b)	Simulation (c)	Simulation (d)
n_p (10^{16} cm^{-3})	5.66	5.66	2.0	2.0
N_b ($10^{10}e^-$)	0.02/0.12	6/24	0.018	0.9
σ_r ($10^{-3}c/\omega_p$)	9.09	89.8	5.3	13
L (c/ω_p)	4.91/11.4	4.91/8.72	3.72	3.72
Θ (10^{-3} rad)	1.96	7.69	4.17	4.17
$r_{\text{blow-out}}$ (c/ω_p)	0.23	4.3	0.24	1.5
c_τ	$\sim$1	$\sim$1	[a]vary w/ξ	[a]vary w/ξ
c_ψ	$\sim$1	$<$1	$\sim$1	$<$1

[a]See text.

$$(1+\psi_0)[\psi_0' r_1' + (1+\psi_0) r_1'' + (E_0 - V_0 B_0) r_0' r_1'] = -\gamma_0 (E_1 - V_0 B_1 - V_1 B_0). \tag{8}$$

After substituting the value for $(E_0 - V_0 B_0)$ from Eq. (7) into Eq. (8) and dividing by $(1+\psi_0)^2$, one finds

$$r_1'' + \{\psi_0'(1+\psi_0)^{-1} - \gamma_0^{-1}[(1+\psi_0) r_0'' + \psi_0' r_0']r_0'\} r_1' = -\gamma_0 (1+\psi_0)^{-2}(E_1 - V_0 B_1 - V_1 B_0). \tag{9}$$

Equation (9) is a second order ordinary differential equation for r_1 with coefficients depending on the zeroth order quantities and their ξ derivatives. The first two terms in the last bracket on the right-hand side $-(E_1 - V_0 B_1)$ are the sum of the perturbation force from the displacement of the beam, F_{b1}, and the change in the plasma self-force due to the displacement of the sheath, F_{e1}. The former can be expressed as $F_{b1} = -(E_{b1} - V_0 B_{b1})$, where E_{b1} and B_{b1} are the change to the electric and magnetic fields from the beam when the centroid is shifted by x_b, i.e.,

$$E_{b1} = B_{b1} = -\tfrac{1}{2} n_b R_b^2 [(r_0 + r_1 - x_b)^{-1} - r_0^{-1}]. \tag{10}$$

Therefore, $F_{b1} = -(E_{b1} - V_0 B_{b1}) \approx \frac{1}{2} n_b R_b^2 (1 - V_0) \times (x_b - r_1)/r_0^2$ when $|x_b - r_1| \ll r_0$. Evaluating F_{e1} from the actual displacement of the channel would be more complicated. We argue, however, that to lowest order it can be neglected. Under the assumption (confirmed by simulation) that the channel shape does not change significantly then $\phi_1 \approx A_{z1} \approx 0$; thus $F_{e1} = E_{x1} - V_0 B_{y1} = -(1 - V_0)\partial_\xi A_{x1}$, where A_{x1} is the perturbation to the x component of the vector potential, and A_{x1} satisfies $-\nabla_\perp^2 A_{x1} = 4\pi J_{x1}$ with J_{x1} being a first order term in r_1. To lowest order, $A_{x1}(y=0) \approx f[r_0(\xi)] r_1 V_{x0}$, where V_{x0} is the magnitude of the velocity in the $\hat{x}$ direction for an electron at the channel boundary. $F_{e1} = -(1 - V_0)\partial_\xi A_{x1}$ can now be neglected because $V_{x0} \ll 1$ in much of the channel and because we are interested in the "short pulse" for which $\partial_\xi r_0/r_0 \approx 1/r_0 \ll \partial_\xi r_1/r_1$.

The last term $V_1 B_0$ in Eq. (9) can be expressed in terms of r_1 by noting that if $\psi_1 = 0$ then $V_1 = \gamma_1 (1 - V_0)\gamma_0^{-1}$, $\gamma_1 = (1+\psi_0) r_0' r_1'$, and $B_0 = -\frac{1}{2} n_b R_b^2 r_0^{-1} = -\frac{1}{2}\Lambda r_0^{-1}$, giving $V_1 B_0 = -\frac{\Lambda}{2} r_0^{-1} (1+\psi_0)^2 \gamma_0^{-2} r_0' r_1'$ which is proportional to r_1'. Next we drop all the r_1' terms in Eq. (9) because ψ_0', ψ_0'/ψ_0, r_0'', $r_0'/r_0' \ll r_1''/r_1'$ in the "short-pulse" limit. Therefore, Eq. (9) can be written as

$$r_1'' + c_r c_\psi \omega_0^2 r_1 = c_r c_\psi \omega_0^2 x_b, \tag{11}$$

where $c_r \equiv n_b R_b^2/r_0^2 = r_{\text{neu}}^2/r_0^2$ and $c_\psi \equiv 1/(1+\psi_0) = 1/[\gamma_0(1 - V_0)]$ now both vary along the trajectory. Equation (11) is for the upper trajectory $r_+ = r_0 + r_1$. For the lower trajectory $r_- = r_0 + r_2$, r_2 satisfies a similar equation. So $x_c = (r_+ - r_-)/2 = (r_1 - r_2)/2$ satisfies

$$x_c'' + c_r c_\psi \omega_0^2 x_c = c_r c_\psi \omega_0^2 x_b. \tag{12}$$

The equation for beam centroid is the same as Eq. (1).

The differences between Eq. (12) and (1) are c_r, c_ψ. In the adiabatic nonrelativistic limit, $V_{x0} \approx 0$, $r_0 \approx r_{\text{neu}}$, $V_0 \ll 1$; hence $c_r \approx 1$, $\psi_0 \approx 0$, and $c_\psi \approx 1$. Therefore, we recover the result in [4], i.e., Eq. (1). For more intense beam-plasma interactions: (1) the channel radius varies along the beam; (2) the relativistic mass changes the plasma electron resonant frequency and the magnetic field is important due to large V_0. These two effects change the coefficients c_r and c_ψ, respectively, thereby changing the

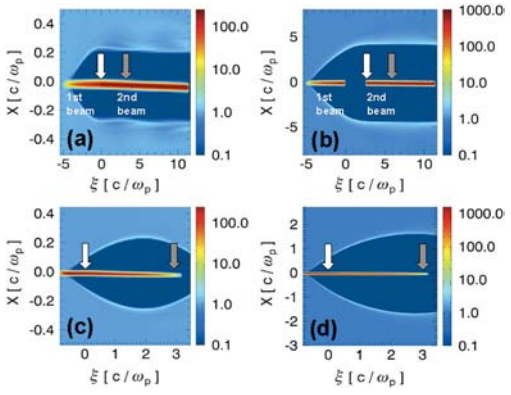

FIG. 2 (color). The beams (red, moving to the left) and the plasma (blue) in (a) the adiabatic nonrelativistic regime, (b) the adiabatic relativistic regime, (c) the nonadiabatic nonrelativistic regime, (d) the nonadiabatic relativistic regime. Left-hand (white) and right-hand (gray) arrows denote where tilts are added and the centroids are measured.

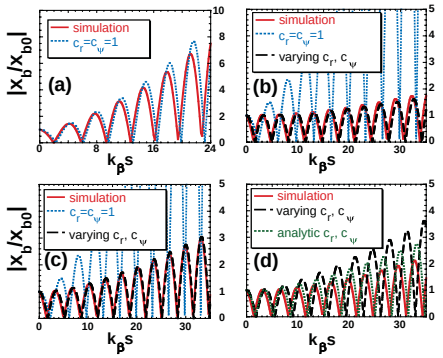

FIG. 3 (color). Hosing growth in four regimes. x_{b0} is the initial displacement of the beam centroid. We assume $\Delta_s = 0.1r_0$, $\Delta_L = 1c/\omega_p$ for the analytic curve in case (d). The slightly slower hosing growth in simulation (d) is caused by nonlinearity in beam-channel centroid coupling.

hosing growth. Generally, $c_r c_\psi < 1$ in a nonadiabatic relativistic channel, therefore reducing hosing growth.

To verify this new hosing theory and to study the effects of c_r and c_ψ, we conduct QuickPIC simulations in the (a) adiabatic nonrelativistic regime, (b) the adiabatic relativistic regime, (c) the nonadiabatic nonrelativistic regime, and (d) the nonadiabatic relativistic regime, respectively. Table I summarizes the parameters and the roles of c_r and c_ψ and Fig. 2 shows the initial beam and the shape of the channel in these simulations. In case (a) and (b), a non-evolving beam is used to create an initial channel, while the trailing beam propagates in an adiabatic (long flat) channel with $r_0 \approx r_{\rm neu}$ and $c_r \approx 1$. In case (c) and (d), a beam with a triangular longitudinal profile creates its own channel. The beam density reaches its peak at $0.27c/\omega_p$ from the head so the ion channel radius varies significantly (non-adiabatically) along the beam but for most part $r_0 > r_{\rm neu}$ and $c_r < 1$. Futhermore, the beams in case (b) and (d) have more charge than in case (a) and (c), resulting in relativistic channels with larger r_0 and $c_\psi < 1$ (see Table I). To trigger the hosing instability, a small linear tilt with angle Θ is imposed on the second beam for case (a) and (b) and at $0.8c/\omega_p$ for case (c) and (d), with the head of the beam on axis and the tail off axis. The beam centroid oscillations at $3c/\omega_p$ behind from where the tilts are added are plotted as solid red curves in Fig. 3 for all four regimes.

We take zeroth order quantities from simulations and numerically integrate Eq. (12) and the beam equation from (1). The results [dashed black curves in Figs. 3(b)–3(d)] agree well with the simulations, while the standard theory [dotted blue curves labeled $c_r = c_\psi = 1$ in Fig. 3, not shown in 3(d)] overestimates the hosing by 1 order of magnitude except for case (a). Therefore, the relatively low hosing growth rate is no longer an anomaly, and our simple model can now be used with confidence to discuss future projects.

In [8] an approximate but analytic model, resulting in Eqs. (10), (11) of [8], was created and used. Using an approximate sheath layer width Δ_s and linear response layer width Δ_L, this model relates ψ to r_0, involving a complicated parameter $\beta(r_0, \Delta_s, \Delta_L)$ [as defined between Eqs. (10), (11) of [8]]. From this model one also has the useful result $\psi_0 = \beta r_0^2/4$; thus $c_\psi = 1/(1 + \beta r_0^2/4)$ is small for large r_0, i.e., the relativistic limit. This model can also be used to directly calculate c_r and c_ψ rather than going through simulation. The result [dotted green curve labeled as "analytic" in Fig. 3(d)] works well comparing with the simulation.

Assuming constant c_r and c_ψ, our theory predicts x_b/x_{b0} has the same asymptotic expression in the "short-pulse" limit as the standard theory result but with $A = 1.3[c_r c_\psi (k_\beta s)(\omega_0 \xi)^2]^{1/3}$. Clearly, reducing the bunch length is still the most effective way to suppress hosing, while the nonadiabatic relativistic regime is advantageous because typically $c_r c_\psi = r_{\rm neu}^2 r_0^{-2}(1 + \beta r_0^2/4)^{-1} \sim O(0.1)$. Therefore, the propagation distance can be made about 10 times longer for the same tolerance of hosing growth. In the recent E167 experiment [2], the beam had $N_b = 1.8 \times 10^{10}$ electrons, spot sizes of $\sigma_r = 10$ μm, a bunch length (in ξ) of $\sigma_z = 15$ μm, and $\gamma_b = 82, 192$. $k_\beta s = 205$ for 85 cm long plasma at $n_p = 2.7 \times 10^{17}$ cm^{-3}. Assuming a constant blow-out radius, we obtain $c_r \approx 0.25$, $c_\psi \approx 0.54$. Thus A is reduced from 7.7 to 3.95 and x_b/x_{b0} is reduced from 35 to only 2.3 for $\omega_0 \xi = 1$ [13].

Last, our theory indicates that the hosing growth rate depends on the beam parameters. When I_b increases, c_r and c_ψ both decrease, thereby reducing hosing growth. Furthermore, the hosing amplitude is not amplified between the drive/trailing beams where $c_r = 0$. These conclusions may help designing more stable PWFA experiments.

Work was supported by DOE under Contracts No. DE-FC02-01ER41179, No. DE-FG02-03ER54721, No. DE-FG03-92-ER40727, No. DE-FG02-03NA00065, No. DE-FG02-97ER41039, No. DE-FG02-92ER40745, and No. DE-FC02-01ER41192, and by NSF under Grant No. PHY0317271. Simulations were performed at local Dawson cluster and NERSC.

[1] M. Hogan *et al.*, Phys. Rev. Lett. **95**, 054802 (2005).
[2] I. Blumenfeld *et al.*, Nature (London) **445**, 741 (2007).
[3] W. P. Leemans *et al.*, Nature Phys. **2**, 696 (2006).
[4] D. H. Whittum *et al.*, Phys. Rev. Lett. **67**, 991 (1991).
[5] J. Krall *et al.*, Phys. Plasmas **2**, 1326 (1995).
[6] A. A. Geraci *et al.*, Phys. Plasmas **7**, 3431 (2000).
[7] M. Lampe *et al.*, Phys. Fluids B **5**, 1888 (1993).
[8] W. Lu *et al.*, Phys. Rev. Lett. **96**, 165002 (2006).
[9] E. S. Dodd *et al.*, Phys. Rev. Lett. **88**, 125001 (2002).
[10] C. Huang *et al.*, J. Comp. Phys. **217**, 658 (2006).
[11] S. Deng *et al.*, Phys. Rev. Lett. **96**, 045001 (2006).
[12] P. Mora *et al.*, Phys. Plasmas **4**, 217 (1997).
[13] In the experiment, σ_r is comparable to r_c, which further reduced the growth rate. See [2].